Journal of Materials Chemistry A

PAPER

View Article Online
View Journal | View Issue

Cite this: J. Mater. Chem. A, 2017, 5, 22576

Consecutive interlayer disassembly–reassembly during alumination of UOV zeolites: insight into the mechanism†

Valeryia Kasneryk,[a] Maksym Opanasenko,*[b] Mariya Shamzhy,[b] Zuzana Musilová,[a] Yamini S. Avadhut,[c] Martin Hartmann[c] and Jiří Čejka[a]

Received 8th July 2017
Accepted 2nd October 2017

DOI: 10.1039/c7ta05935c

rsc.li/materials-a

Investigation of the kinetics of **UOV** germanosilicate alumination by X-ray diffraction, ^{27}Al and ^{29}Si MAS NMR, ICP/OES and FTIR spectroscopy showed the multi-stage mechanism of the process. The first step consists of degermanation and partial disassembly followed by Al incorporation into the **UOV** germanosilicate framework in the second step. The Al atoms stabilize the **UOV** framework by healing the defects formed after rapid hydrolysis of Ge–O–Si bonds, which was evidenced by comparison with the reference treatment of initial **UOV** samples with HNO_3 (pH = 2). Post-synthesis alumination of **UOV** leads to the generation of strong Brønsted and Lewis acid sites; their ratio in aluminated **UOV** derivatives can be adjusted by the variation of treatment conditions. The intrinsic properties of parent **UOV** germanosilicates determine the textural properties of aluminated derivatives.

Introduction

Since 1962, when zeolites were first applied as main components of FCC catalysts by Mobil, they have become key materials for industrial use. Application of zeolites and zeolite related materials covers the areas of heterogeneous catalysis, separation, adsorption and ion exchange.[1] Recently, their use was also expanded to medicine, luminescence, microelectronics,[2] *etc.* The acidic and sorption properties of zeolite materials are determinants of the mentioned applications and strongly depend on their structure and chemical composition controlled in particular by the nature of framework elements (T-element, T = Al, Si, B, Ge, Ti, *etc.*).[1] Most of the zeolites have a special range of T-elements, in which the target phase can be formed.

The big impulse in the discovery of new zeolite structures was given when germanium was first used as an additional framework element.[3] Several new zeolites were synthesized as germanosilicates and germanates: **BEC**,[3] **IWR**,[4] **ITH**,[5,6] **ITR**,[7] **IWW**,[8] and **IWS**,[9] including extra-large pore zeolites **UTL**,[10,11] **IRR**,[12] **-IRY**,[13] and **ITQ-43**,[14] *etc.* The presence of germanium atoms in reaction gels is essential, as they play the role of an inorganic structure directing agent (SDA) particularly forming double-four-ring (D4R) and double-three-ring (D3R) building units.[3,12,15,16] Also they accelerate the crystallization process[17,18] and stabilize the frameworks of these materials.[17,19] At the same time, Si–O–Ge and Ge–O–Ge bonds are easily hydrolysable even by atmospheric moisture. Recently, this feature of germanosilicate zeolites in combination with the preferential occupation of D4R by Ge atoms was perfectly used for the development of the ADOR (Assembly–Disassembly–Organization–Reassembly) methodology for the design of novel zeolites.[20–22] Based on the zeolite **UTL** possessing dense Si-rich layers linked by Ge-rich D4Rs, a new family of zeolites was synthesized: IPC-2 (with **OKO** topology), IPC-4 (with **PCR** topology),[20] and "unfeasible" zeolites IPC-9 and IPC-10.[23]

Ge atoms can be simply extracted from zeolite frameworks[24–26] as well as post-synthetically isomorphously substituted by different elements. Post-synthesis alumination was previously demonstrated for germanosilicates with **IWW**,[27] **IWR**,[28] **ITH**[29,30] and **BEC**[31] topologies. Al incorporation into the frameworks of these zeolites allowed the (i) generation of strong acid centers, (ii) increase of the hydrolytic stability of the framework and (iii) formation of additional mesopores, which lead altogether to the design of hierarchically porous catalysts. The intrinsic properties of the initial material as well as the conditions of the treatment were shown to be important parameters controlling the amount of formed acid centers and the micro-/mesopore ratios. Previously it was observed that zeolites directly synthesized from Al–Si–Ge reaction mixtures can only be obtained in a quite narrow range of Si/T-element ratios.[32] On the other hand, post-synthesis alumination allowed expanding this range, which can also be considered as an advantage of this method. The obtained

[a]J. Heyrovský Institute of Physical Chemistry, Academy of Sciences of the Czech Republic, Dolejškova 3, 182 23 Prague 8, Czech Republic

[b]Department of Physical and Macromolecular Chemistry, Faculty of Science, Charles University, Hlavova 8, 128 43 Prague 2, Czech Republic. E-mail: maksym.opanasenko@jh-inst.cas.cz

[c]Erlangen Catalysis Resource Center, Friedrich-Alexander-Universität Erlangen-Nürnberg (FAU), Egerlandstraße 3, 91058 Erlangen, Germany

† Electronic supplementary information (ESI) available. See DOI: 10.1039/c7ta05935c

aluminogermanosilicate materials were investigated in tetrahydropyranylation of alcohols[28,29] and aromatic hydrocarbon alkylation[33] as model reactions. In addition to alumination, the possibility of post-synthesis introduction of Ga was described for **IWR** germanosilicates.[28] Final materials showed high catalytic activity in the acylation of *p*-xylene with benzoyl chloride reaction. Furthermore, Xu *et al.* showed the way of post-synthesis Ge substitution by Si atoms,[34] which resulted in an increase of hydrolytic stability of **UTL**, **UWY**, **BEC** and **IWR** germanosilicates.

Recently, Lorgouilloux *et al.* reported the synthesis of a new germanosilicate **UOV**.[35] It possesses a 3-dimensional pore system composed of large 12- (7.7 × 6.0 Å and 5.9 × 7.1 Å) and small 8- (2.9 × 3.1 Å) ring channels along the [100] direction intersected by 10-ring (5.9 × 4.7 Å) pores along [001]. This zeolite was synthesized from concentrated reaction gels (H_2O/T < 10, T = Si + Ge) and with Si/Ge = 0.5–4.[35,36] Recently, we showed the possibility of the ADOR transformation for this zeolite,[36] which was the first example of successful application of materials with porous layers using this methodology. As a result, new zeolite IPC-12, which possesses the same topology of the layers as **UOV** but different connectivity between layers, was obtained.

In this work, we focused on the process of post-synthesis alumination of **UOV** germanosilicates. Although there were numerous reports covering the process for germanosilicate materials and related investigations of their acidic and catalytic properties, no attention was paid to the mechanism of Ge-to-Al substitution. Previously, it was assumed that the process is consecutive, *i.e.* degermanation followed by alumination. In order to prove or disprove this hypothesis, we deeply investigated the kinetics of Al incorporation into the **UOV** framework using X-ray diffraction and ^{27}Al and ^{29}Si MAS NMR and ICP/OES methods. Moreover, we studied the influence of the chemical composition of the parent zeolite as well as the conditions of post-synthesis alumination on the structural and acidic properties of aluminated **UOV** derivatives.

Experimental part

Materials

Decamethonium bromide (>98.0%, TCI), germanium oxide (99.99%, Sigma Aldrich), Cab-O-Sil M5 (Supelco Analytical), aluminum hydroxide (Sigma Aldrich), methanol (99.98%, Lachner), acetone (99.97%, Lachner), aluminum nitrate nonahydrate (≥98.5%, Sigma Aldrich), and nitric acid (>70%, Sigma Aldrich) were used for the synthesis and post-synthesis modification of **UOV** zeolites.

Hydrofluoric acid (48 wt% in H_2O, ANALPURE®), nitric acid (67 wt% in H_2O, ANALPURE®), hydrochloric acid (36 wt% in H_2O, ANALPURE®) supplied by Analytika, and boric acid (>99.5%, Sigma) were used for the decomposition of zeolites.

Syntheses of UOV zeolites

Germanosilicate **UOV** samples were obtained according to ref. 35 from the reaction mixtures with the following composition: xSiO$_2$: $(1 - x)$GeO$_2$: 0.25DMDH : 10H$_2$O, where x = 0.33 or 0.66, using decamethonium dihydroxide (DMDH) as SDA. Decamethonium dihydroxide was prepared from the bromide form by ion exchange using Ambersep® 900(OH) anion exchange resin (0.4 mmol of SDA per 1 g of anion exchange resin). The solution of DMDH was concentrated under low pressure (25 torr) at 30 °C until the hydroxide concentration exceeded 1.5 mol l^{-1}. For **UOV** synthesis, the given amount of germanium oxide was dissolved in an aqueous solution of DMDH. Silica (Cab-O-Sil M5) was gradually added into the solution, and the mixture was stirred at room temperature for 30 min. Thereafter, the reaction gels were autoclaved at 175 °C for 7–14 days under static conditions. The solid product was recovered by centrifugation, washed several times with distilled water (until the pH of washing solution was ~7), dried at 65 °C for 12 h and finally calcined at 550–750 °C for 6 h with a temperature ramp of 2 °C min^{-1} under air flow (200 ml min^{-1}). The prepared **UOV** samples are denoted as **UOV**-n, where n is the Si/Ge ratio in the starting reaction mixture.

Aluminum-containing samples were prepared from initial starting gels with compositions: xSiO$_2$: $(1 - x)$GeO$_2$: 0.005Al$_2$O$_3$: 0.25DMDH : 10H$_2$O, where x = 0.33 or 0.6, using the same procedure and adding aluminum hydroxide in the reaction mixture. The final samples were named Al-**UOV**-n, where n is the Si/Ge ratio in the starting reaction mixture.

Post-synthesis treatment

(a) Post-synthesis alumination of **UOV** zeolites was performed by:

- Stirring of the parent **UOV** zeolite in 1 mol l^{-1} solution of Al(NO$_3$)$_3$ (1 g of zeolite per 100 ml of solution) at T = 80 °C and pH = 2.0 for 5 min to 15 days.
- Treatment of the **UOV** germanosilicate zeolite in a 1 mol l^{-1} solution of Al(NO$_3$)$_3$ (1 g of zeolite per 100 ml of solution) at T = 175 °C and pH = 2.0 for 24 h in an autoclave.

Aluminated samples are designated as **UOV**-n-alumination temperature-alumination time.

(b) Post-synthesis acidic treatment of **UOV** zeolites was done by stirring the parent **UOV** zeolite in a 0.01 mol l^{-1} solution of HNO$_3$ (1 g of zeolite per 100 ml of solution) at T = 80 °C and pH = 2.0 for 24 h.

Characterization

The structure and crystallinity of zeolites under study were determined by X-ray powder diffraction (XRD) using a Bruker AXS-D8 Advance diffractometer with a graphite monochromator and a position sensitive detector (Våntec-1) using CuKα radiation in Bragg–Brentano geometry at a scan rate of 0.25° (2θ per min).

The chemical compositions of **UOV** samples were determined by ICP/OES (ThermoScientific iCAP 7000) analysis. 50 mg of zeolite were mineralized in a mixture of 2 ml of 48% HF, 4 ml of 67% HNO$_3$, and 4 ml of 36% HCl in a microwave. After cooling, the excess HF was eliminated by complexation with 15 ml of a saturated solution of H$_3$BO$_3$ and the final mixture was

treated in a microwave again. Thereafter, the solutions under analysis were collected and diluted with ultrapure water to a total volume of 250 ml.

The size and shape of **UOV** crystals were studied by scanning electron microscopy (SEM, JEOL JSM-5500LV microscope). For the measurement the crystals were coated with a thin layer of platinum (~10 nm) in a BAL-TEC SCD-050 instrument.

Nitrogen adsorption/desorption isotherms were measured using an ASAP 2020 (Micromeritics) static volumetric apparatus at liquid nitrogen temperature (−196 °C). Prior to the sorption measurements, all samples were degassed with a turbomolecular pump at 300 °C for 8 h. The specific surface area (S_{BET}) was evaluated by the BET method[37] using adsorption data in the p/p_0 range of 0.05–0.20. The *t*-plot method[38] was applied to determine the volume of micropores (V_{micro}). The volume of mesopores in the range from 5 to 20 nm was calculated from the desorption branch of the isotherm using the BJH method with the Halsey equation.

The concentrations of Lewis (c_L) and Brønsted (c_B) acid sites were determined after the adsorption of pyridine (Py) by FTIR spectroscopy using a Nicolet 6700 with a transmission MCT/B detector. The zeolites were pressed into self-supporting wafers with a density of 8.0–12 mg cm^{-2} and activated *in situ* at T = 450 °C and $p = 5 \times 10^{-5}$ torr for 4 h. Pyridine adsorption was carried out at 150 °C and a partial pressure of 3.5 torr for 20 min followed by desorption for 20 min at the same temperature. Before adsorption, pyridine was degassed by freeze–pump–thaw cycles. All spectra were recorded with a resolution of 4 cm^{-1} by collecting 128 scans for a single spectrum at room temperature. The spectra were recalculated using a wafer density of 10 mg cm^{-2}. c_L and c_B were evaluated from the integral intensities of bands at 1454 cm^{-1} (c_L) and 1545 cm^{-1} (c_B) using extinction coefficients, $\varepsilon(L) = 2.22$ cm μmol^{-1} and $\varepsilon(B) = 1.67$ cm μmol^{-1}.[39] For the determination of the strength of different acid sites, desorption of pyridine was carried out at 150, 250, 350 and 450 °C followed by FTIR measurements.

The solid state ^{27}Al and ^{29}Si Magic Angle Spinning (MAS) NMR spectra were recorded on an Agilent DD2 500WB spectrometer at resonance frequencies of 130.24 and 99.30 MHz, respectively. All MAS NMR experiments were carried out with a commercial 3.2 mm triple resonance MAS probe. The chemical shifts of ^{29}Si are referenced to tetramethylsilane (TMS) at 0 ppm and those of ^{27}Al are referenced to a 1.1 mol kg^{-1} solution of $Al(NO)_3$ in D_2O on a deshielding scale. Saturation combs were applied prior to all repetition delays. All ^{27}Al MAS spectra were recorded using single pulse excitation (1D) at a sample spinning frequency of 15 kHz. Typical 90° pulse lengths for the ^{27}Al central transition were 1.25 μs and recycle delays of 1.0–15.0 s. Similarly, ^{29}Si 1D experiments were acquired at a sample spinning frequency of 10 kHz using a pulse length of 3 μs and a recycle delay of 60 s. During the ^{29}Si acquisition period proton broadband decoupling was applied with a continuous wave sequence using a nutation frequency of 100 kHz. In total 6000 and 1000 numbers of scans were acquired for ^{27}Al and ^{29}Si, respectively. $^{29}Si\{^1H\}$ spectra based on ramped cross-polarization (CP) with magic angle spinning (CP-MAS) were acquired at a sample spinning frequency of 6 kHz with a recycle delay of 5.0 s and a contact time of 5.0 ms.[42]

Results and discussion

Syntheses of parent UOV and Al-UOV zeolites

Parent germanosilicate **UOV** samples were synthesized from reaction gels with Si/Ge = 0.5 and 1.5. The obtained samples were highly crystalline single-phase materials with the **UOV** topology (Fig. 1A and B).[35] Despite the significant difference in the Ge concentration of starting reaction gels, final samples possess comparable Si/Ge ratios: 2.3 and 3.1 for **UOV**-0.5 and **UOV**-1.5, respectively (ESI, Table S1†). The discrepancy in the chemical composition between starting gels and final samples is explained by the "saturation" of available T-sites in the framework with Ge atoms similar to those discussed in ref. 40 and 41. In addition, the chemical composition of starting reaction gels influenced the morphology of formed **UOV** crystals. While the Ge-rich **UOV**-0.5 sample was characterized by tiny ellipsoid crystals with a size of 0.3 μm × 0.3 μm × 0.1 μm (Fig. 2A), the Ge-poor **UOV**-1.5 sample exhibits 3-times larger crystals (1 μm × 0.9 μm × 0.2 μm, Fig. 2D). A similar increase in the crystal size with decreasing Ge amount in the reaction mixture probably related to the change in the nucleation rate was previously shown for the germanosilicates with the **ISV** topology.[18]

Direct incorporation of aluminum into the **UOV** framework was performed using initial gels with the same Si/Ge ratios (0.5 and 1.5) in the presence of 1 mol% Al. The XRD patterns of the resulting Al-**UOV**-*n* confirmed that the obtained samples are single phase materials without an admixture of the Al_2O_3 phase (Fig. 1C). Similar to **UOV** samples, Al-**UOV**-*n* materials were characterized by comparable Si/Ge ratios (4.8–5.2, Table SI-1†), which increased in comparison with initial mixtures. The presence of aluminum in the initial reaction mixtures resulted in the decrease in the Ge content of the final materials when compared with **UOV**-*n*. The amount of incorporated Al was 0.78% for Al-**UOV**-0.5 and 0.35% for Al-**UOV**-1.5. In both cases **UOV** samples possess tiny plate-like crystals of 1 μm × 1 μm × 0.1 μm in size (Fig. 2G and H).

Evolution of UOV alumination: XRD and ^{27}Al and ^{29}Si MAS NMR studies

Fig. 1B shows the XRD patterns of **UOV** samples subjected to alumination with 1 M $Al(NO_3)_3$ (pH = 2) under different conditions: at 80 °C for 96 h or 175 °C for 24 h. The XRD patterns of aluminated derivatives display sharp diffraction lines at characteristic 2θ positions evidencing the preservation of the **UOV** structure after the treatments and the absence of $Al(NO_3)_3$, Al_2O_3 or any other admixtures. The samples aluminated at 175 °C were characterized by lower crystallinity in comparison with parent **UOV**. Such differences can be explained by the reduction of the crystallite size due to the fragmentation of the zeolite particles and partial degradation of the zeolite framework under hydrothermal conditions. These assumptions are supported by SEM images (Fig. 2C and F) showing an increased fraction of cracked crystals after post-synthesis alumination at 175 °C. **UOV**-0.5 and **UOV**-1.5 samples subjected to alumination were characterized by plate-

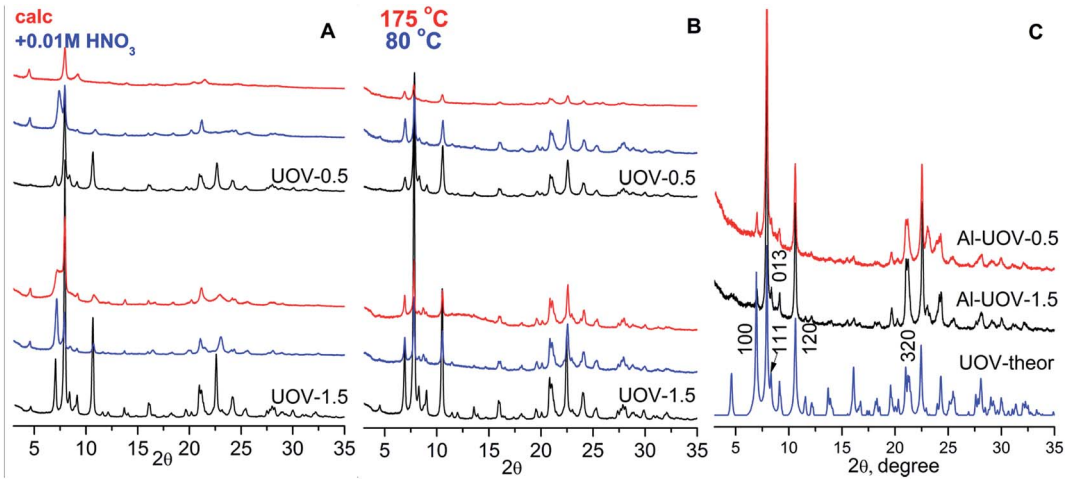

Fig. 1 XRD patterns of (A) **UOV**-1.5 and **UOV**-0.5 samples with 0.01 M HNO_3 (pH = 2) – black – parent **UOV** samples, red – before calcination and blue – after calcination; (B) post-synthesis aluminated **UOV**-1.5 and **UOV**-0.5 samples, black – parent **UOV** samples, blue – 80 °C and 96 h, and red – 175 °C and 24 h; (C) aluminum-containing Al-**UOV**-1.5 and Al-**UOV**-0.5 directly synthesized and the theoretically predicted XRD pattern of **UOV** from the IZA database (interlayer (100), (111), (120) and (320) and intralayer (013) signals are designated).

like crystals with a size of 0.3 μm × 0.3 μm × 0.1 μm and 1 μm × 0.9 μm × 0.15 μm, respectively (Fig. 2B, C, E and F).

In order to compare the behavior of the parent germanosilicate in the presence and absence of Al, we performed the reference treatment of initial **UOV** with HNO_3 at pH = 2. Acidic treatment of **UOV** without Al resulted in a framework transformation as evidenced by the significant broadening and decrease of intensities of all diffraction lines for **UOV**-1.5 or the change of their positions for **UOV**-0.5 (Fig. 1A), as interlayer (100), (111), (120) and (320) signals were less intensive and shifted to the high angle region. This is explained by leaching of Ge atoms from the **UOV** framework resulting in a decrease in the framework density (for **UOV**-1.5) or even full disassembly (for **UOV**-0.5) followed by the formation of the IPC-12 zeolite after calcination. Similar behavior of germanosilicates upon acidic treatment was reported for **IWW** and **ITH** zeolites.[24] Comparison of the results of the treatment with $Al(NO_3)_3$ and HNO_3 evidences that Al atoms stabilize the **UOV** framework by healing the defects formed after rapid hydrolysis of Ge–O–Si bonds. To confirm the assumption of a multistep alumination process, a detailed kinetic study followed by XRD, chemical analysis and ^{27}Al as well as ^{29}Si MAS NMR measurements was performed.

After 5 minutes of the alumination at 80 °C, the interlayer (100) peak (7.08° 2θ) has already shifted to the high-angle region for both **UOV**-0.5 and **UOV**-1.5 samples (Fig. 3). The observed peak shift (shifts: $\Delta = 0.10°$ 2θ for **UOV**-0.5 and $\Delta = 0.19°$ 2θ for **UOV**-1.5 after 5 min) indicates that the structure of building units between the layers was changed at the beginning of the treatment. The XRD patterns of samples after 5 min, 30 min and 3 h of alumination contained additional peaks (16.56° and 24.38° 2θ) corresponding to the lamellar precursor of the IPC-12 material derived from **UOV**[36] (Fig. 1A). Prolongation of the alumination up to 24 h resulted in the disappearance of these diffraction lines due to the restoration of the **UOV** structure. A gradual left-shift displacement of the (100) signal up to the interlayer peak position of parent **UOV** was observed. The XRD patterns of **UOV**-0.5 and **UOV**-1.5 zeolites subjected to alumination for 24 h indicate the presence of the **UOV** single phase (Fig. 3). Prolongation of the treatment up to 7 d and 15 d resulted in a partial destruction of the zeolite framework, as all the XRD lines were less intensive and broader compared with **UOV** samples aluminated for 4 d. Assuming that the intensity of the (020) intralayer signal for **UOV**-*n*-Al-80-24h is 100%, the samples subjected to alumination for >96 h were characterized by the decreased intensities of the (020) line: 7 d – 55% (**UOV**-0.5) and 43% (**UOV**-1.5), while for 15 d – 46% (**UOV**-0.5) and 30% (**UOV**-1.5) (Fig. SI-1†). Moreover, the XRD pattern of the calcined sample **UOV**-0.5-Al-80-5min (ESI, Fig. SI-2†) exhibited broad lines with low intensity and corresponded to a defective **UOV** structure, while the diffractogram of the sample after 4 days of alumination was characteristic of highly crystalline **UOV**. We suppose that at the first step of alumination the acidic hydrolysis of Ge-rich D4Rs and leaching of Ge atoms from the framework take place. Short times of the treatment are inappropriate for the incorporation of Al atoms into the **UOV** framework because in contrast to small protons, which quickly penetrate into the pores and catalyze the hydrolysis, hydrated aluminum cations suffer from relatively high diffusion constraints. With prolongation of the treatment, Al atoms get into the zeolite pores and heal the defects formed after hydrolysis of the Ge-domains. This assumption agrees with the results of ICP/OES analysis (Table SI-1†) showing a significant drop in the Ge concentration (by 2.6–2.9 times) in the framework after 5 minutes of alumination (Table SI-1†). Further leaching of Ge atoms proceeds significantly slower and Ge is still detected in the **UOV** framework even after 15 d. With prolongation of the treatment from 5 min to 96 h, the Al concentration increased from 0.73 to 2.66% for **UOV**-1.5 and from 2.08 to 2.97% for **UOV**-0.5. Prolongation of the treatment

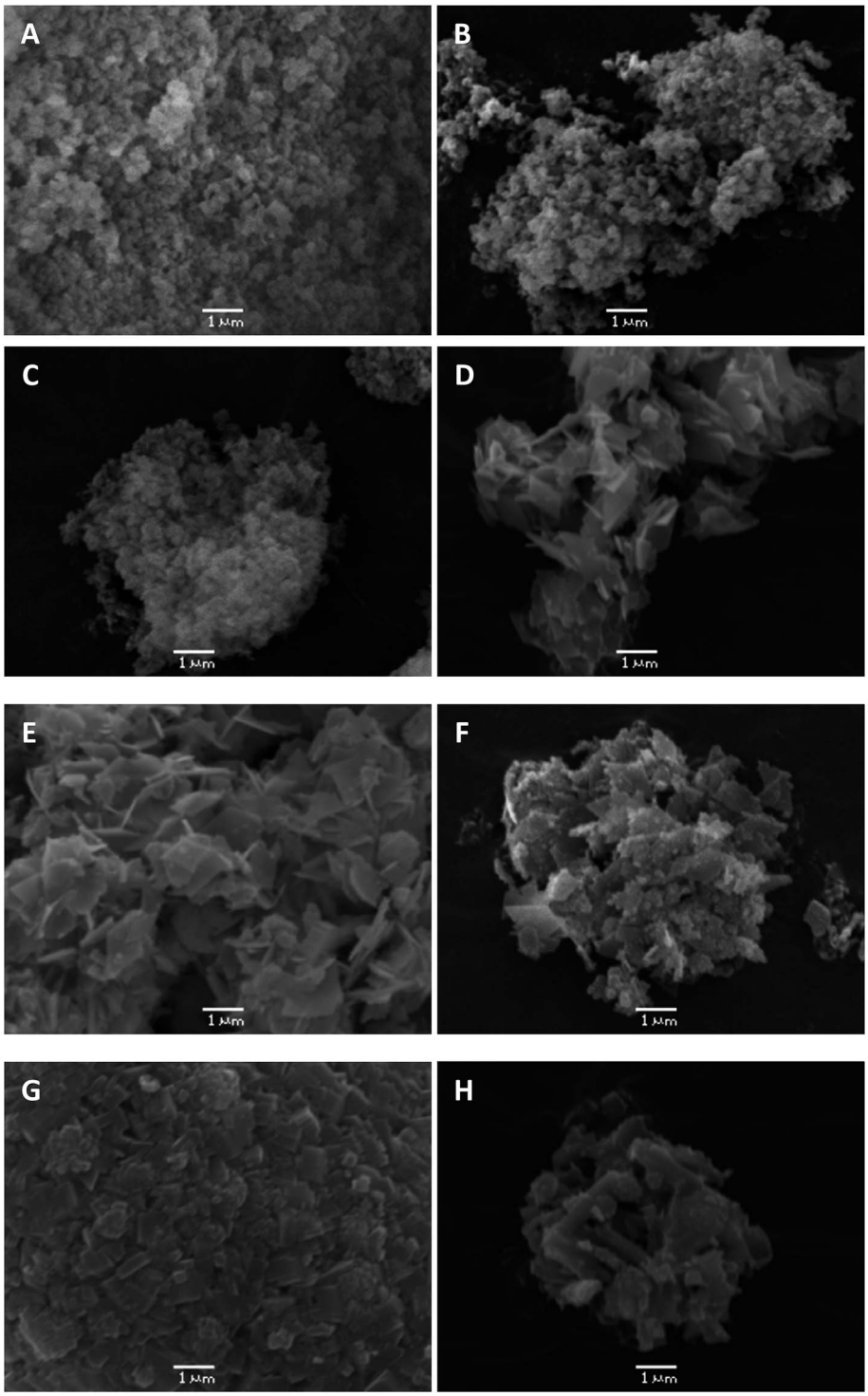

Fig. 2 SEM pictures of: (A) **UOV**-0.5, (B) **UOV**-0.5-80C-96h, (C) **UOV**-0.5-175C-24h, (D) **UOV**-1.5, (E) **UOV**-1.5-80-96h, (F) **UOV**-1.5-175-24h, (G) Al-**UOV**-1.5, and (H) Al-**UOV**-0.5.

up to 7 d and 15 d resulted in a decrease in the Al amount (Table SI-1†), which is in agreement with the results of the XRD. However, the relatively high observable concentration of Al in the samples after 5 min of the treatment does not mean that the aluminum atoms are truly incorporated into the **UOV** framework. Solid-state NMR spectroscopy was used to distinguish the state of Al atoms and to trace the silanol defects (if any) after different alumination times.

The signal at −100 ppm in the ^{29}Si MAS NMR spectrum corresponds to deficient silanol groups (Q^3 silicon atoms). The intensity of this signal decreased with prolongation of the treatment from 5 min to 96 h for the non-calcined aluminated

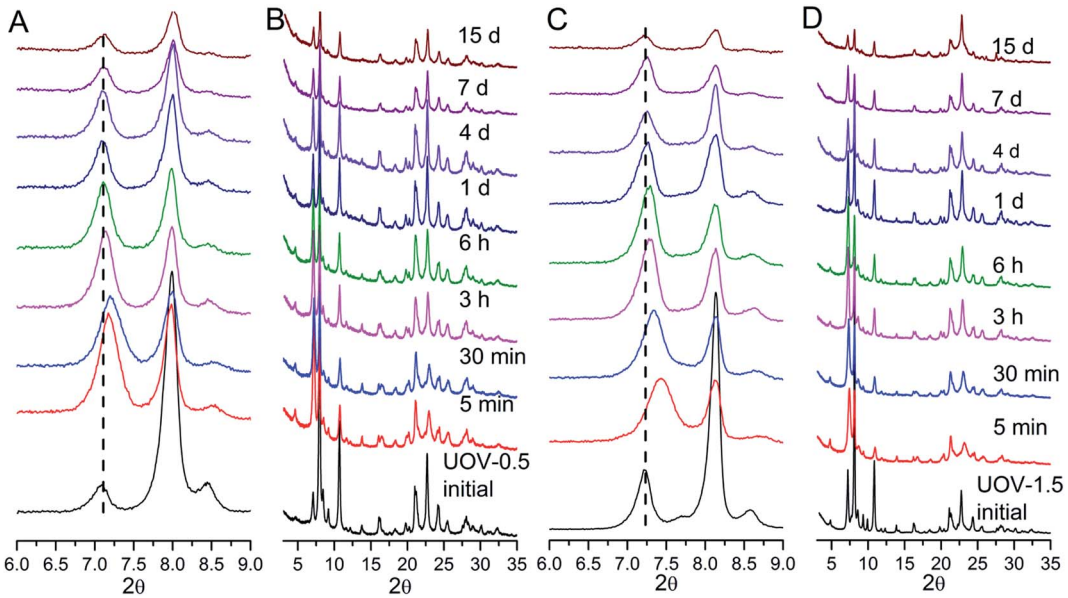

Fig. 3 Kinetic investigation of the alumination procedure at 80 °C: (A) small angle region and (B) full region of XRD patterns of **UOV**-0.5 and (C) small angle region and (D) full region of XRD patterns of **UOV**-1.5. Black dotted lines correspond to the positions of the (100) reflection in parent **UOV** samples.

UOV-0.5 sample (Fig. 4A), which confirms the healing of silanol defects with time. Calcination has a similar effect and the ^{29}Si MAS NMR spectra of **UOV**-0.5-Al-80-5min after calcination were characterized by the presence of a dominant signal at −110 ppm attributed to Q^4 silicon atoms surrounded by 4 Si atoms and a signal of Q^3 Si atoms with significantly decreased intensity (Fig. SI-5 and SI-6† include deconvolution data for spectra clearly showing Q^3 and Q^4 silicon atoms).

All ^{27}Al MAS NMR spectra of aluminated samples show the presence of a signal at 55 ppm corresponding to tetrahedral Al(IV), and a signal at 0.8 ppm with a shoulder characteristic of octahedral Al(VI) species. Calcination of **UOV**-0.5 aluminated at 80 °C for 5 min resulted in a significant decrease in the intensity of the AlO_4 signal accompanied by the appearance of a strong signal of penta-coordinated aluminum at 14 ppm (Fig. 4B). Thus, despite the ICP-OES results showing a remarkably high amount of Al in the sample after 5 minutes of the treatment, most of the aluminum atoms were in the extra-framework and the short time was not sufficient for Al incorporation. In contrast, the intensity of the signal of Al(IV) after calcination was dominant in the spectra of **UOV**-0.5-Al-80-96h (Fig. 4B). This evidences the incorporation of most aluminum atoms into the **UOV** framework.

The chemical composition of the parent **UOV** material is an important parameter for the prevailing direction of aluminum incorporation. The spectra of **UOV**-1.5-Al-80-t samples were

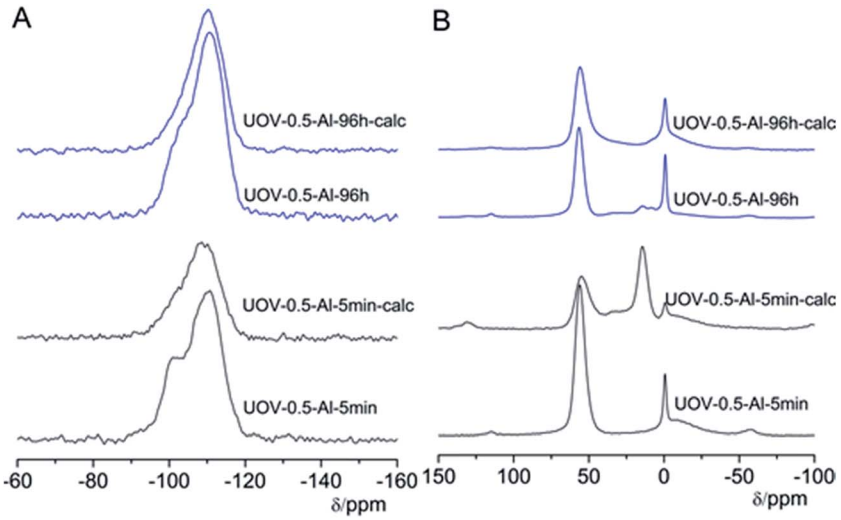

Fig. 4 (A) ^{29}Si MAS NMR and (B) ^{27}Al MAS NMR spectra of **UOV**-0.5 aluminated at 80 °C for 5 min and 96 h before and after calcination.

Table 1 The concentrations of Lewis and Brønsted acid centers in UOV derivatives determined by means of FTIR spectroscopy of adsorbed pyridine

Sample	c (Brønsted sites), mmol g^{-1}	c (Lewis sites), mmol g^{-1}	c (total), mmol g^{-1}
UOV-1.5	0.01	0.03	0.04
UOV-1.5-Al-80-24h	0.17	0.17	0.34
UOV-1.5-Al-80-96h	0.12	0.29	0.41
UOV-1.5-Al-175-24h	0.25	0.17	0.42
Al-**UOV**-1.5	0.10	0.10	0.20
UOV-0.5	0.02	0.03	0.05
UOV-0.5-Al-80-24h	0.10	0.11	0.21
UOV-0.5-Al-80-96h	0.24	0.21	0.45
UOV-0.5-Al-175-24h	0.22	0.18	0.40
Al-**UOV**-0.5	0.11	0.12	0.23

characterized by predominant signals at 55 ppm attributed to Al(IV) (Fig. SI-3†). However, in contrast to **UOV**-0.5-80-96h (Fig. 4B), penta-coordinated aluminum was present in the **UOV**-1.5-80-96 sample, evidencing the presence of a higher amount of extra-framework aluminum atoms. The temperature of the treatment had an impact on Al incorporation as well. Thus, despite the high concentration of Al in samples treated at 175 °C, ^{27}Al MAS NMR analysis of **UOV**-*n*-Al-175-24h (Fig. SI-4†) samples showed the presence of intense signals of octahedral (VI) (0.8 ppm) and penta-coordinated (V) (14 ppm) aluminum indicating that Al atoms are not incorporated into the framework.

According to the ICP-OES analysis, directly synthesized Al-**UOV**-*n* possessed a lower amount of aluminum in comparison with post-synthesis aluminated samples (ESI, Table 1). ^{27}Al MAS NMR analysis (Fig. 5A) showed the presence of 2 signals: sixfold-coordinated extra-framework aluminum species (0.8 ppm) and tetrahedrally coordinated (55 ppm) aluminum atoms. In the case of the Al-**UOV**-0.5 sample predominant signals were related to extra-framework AlO_6 species. This result can be considered as an advantage of post-synthesis alumination in comparison with direct synthesis of Al-**UOV** resulting in the incorporation of a limited amount of aluminum.

In order to compare the coordination of Si atoms, the ^{29}Si{^{1}H} CP-MAS NMR spectra (Fig. 5B) of **UOV**-0.5, **UOV**-0.5 aluminated at 80 °C for 96 h and directly synthesized aluminum containing Al-**UOV**-0.5 were obtained. The spectrum of **UOV**-0.5 was characterized by the presence of 2 signals: at −100.6 ppm and −109.0 ppm corresponding to Q^3 and Q^4 silanol atoms, respectively. Alumination of this sample resulted in the formation of defects, as the intensity of the signal Q^3 atoms was significantly increased. This was also accompanied by the decrease in the Q^4 signal intensity, as well as by the formation of Q^2 silanol defects (−91.7 ppm). Similar to post-synthesis aluminated **UOV**-0.5, the dominant signal for directly synthesized Al-**UOV**-0.5 was the one attributed to Q^3 silanol groups. Moreover, the signals of Q^4 Si atoms at −111.0 and −114.0 ppm were present in the spectrum of Al-**UOV**-0.5. Thus, the way of alumination significantly influences the coordination of silicon atoms in the zeolite framework.

The nature and concentration of acid centers in Al-containing UOV zeolites: synthesis *vs.* post-synthesis incorporation of Al

We studied the evolution of hydroxyl groups in Ge-rich and Ge-poor **UOV** samples during alumination using FTIR spectroscopy (Fig. 6I and II). Two adsorption bands were observed in the region of 4000–3200 cm^{-1} in the spectra of parent **UOV**-0.5 and **UOV**-1.5 samples: the band corresponding to silanol groups (at 3745 cm^{-1}) and the broad adsorption band at 3685–3630 cm^{-1} attributed to external Ge-OH groups.

In comparison with parent **UOV**s, the intensity of the band at 3745 cm^{-1} increased for all aluminated samples, which indicates the increased concentration of silanol defects formed due to the breaking of hydrolytically unstable Si–O–Ge bonds. Both **UOV**-0.5 and **UOV**-1.5 samples subjected to hydrothermal alumination (at 175 °C) were characterized by less intensive absorption bands at 3745 cm^{-1} in contrast to the samples treated at 80 °C. In addition, the increasing temperature of alumination from 80 to 175 °C (τ = 24 h) or the prolongation of the treatment from 24 to 96 h (T = 80 °C) resulted in an enhanced intensity of absorption bands at 3620 cm^{-1}, which is characteristic of bridging hydroxyl Si–(OH)–Al groups. These phenomena show that the increase in the temperature

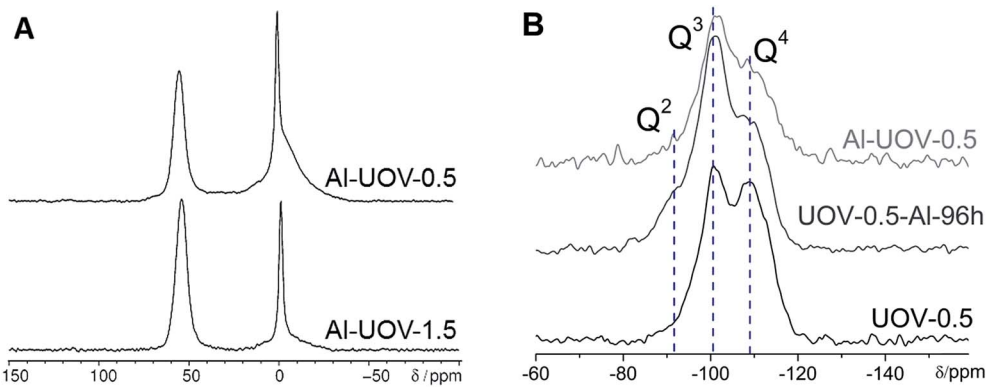

Fig. 5 (A) ^{27}Al MAS NMR directly synthesized Al-**UOV**-*n* samples and (B) ^{29}Si{^{1}H} CP-MAS NMR spectra of **UOV**-0.5, **UOV**-0.5-Al-80-96h-calc and Al-**UOV**-0.5.

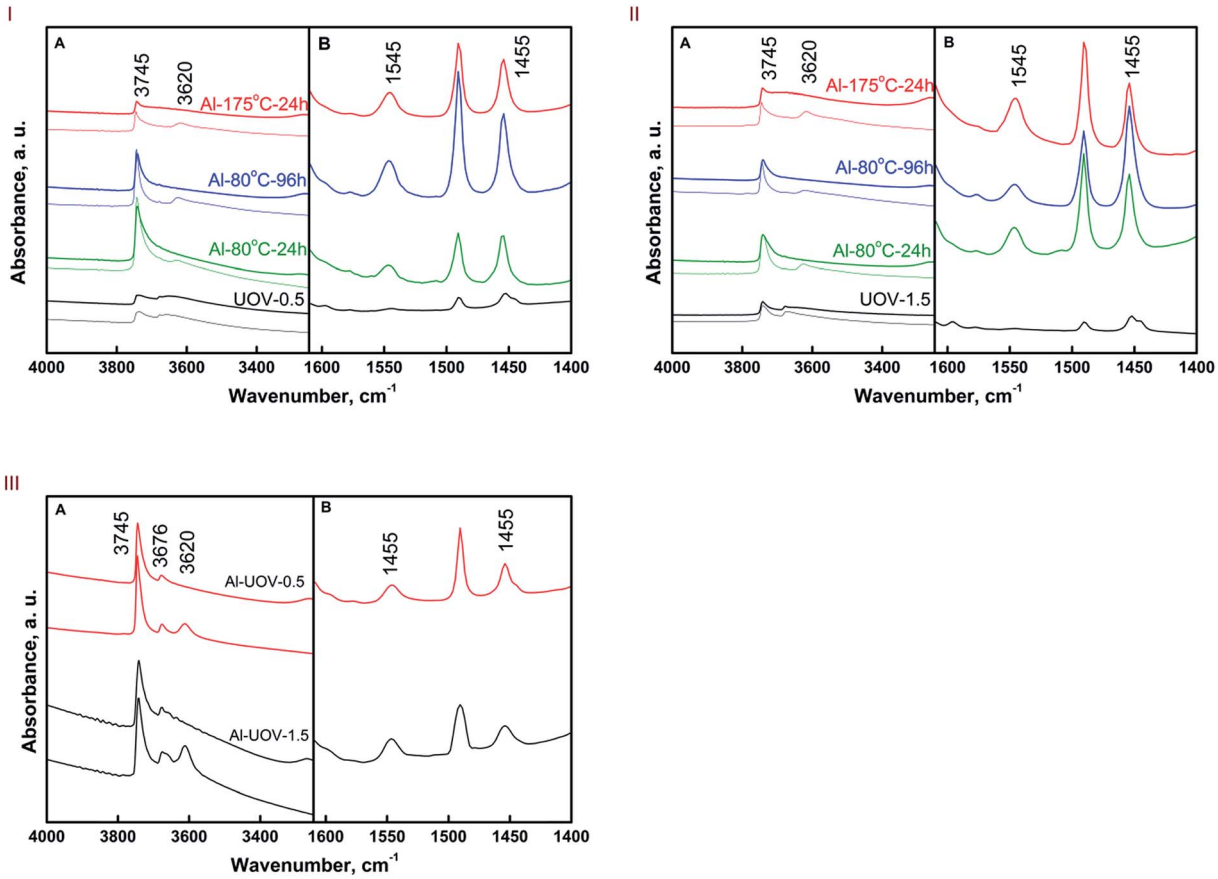

Fig. 6 IR spectra of (I) UOV-0.5 and (II) UOV-1.5 zeolites: parent samples (black), UOV-*n*-Al-80-24h (green), UOV-*n*-80-96h (blue), and UOV-*n*-175-24h (red). (III) Al-UOV-*n*: Al-UOV-1.5 (black) and Al-UOV-0.5 (red). (A) Regions of hydroxyl vibrations; (B) region of pyridine vibrations. Bottom line and top line spectra show the spectra before and after adsorption of pyridine.

accelerated the healing of silanol defects and the incorporation of Al atoms into the framework. A similar effect of the temperature was previously shown for germanosilicate **ITH**.[29] The prolongation of the treatment had the same effect on the incorporation of Al. We observed a simultaneous decrease in the intensity of the signal at 3745 cm^{-1} and increase of the band at 3614 cm^{-1} with prolongation of alumination from 24 h to 96 h at 80 °C. This also agreed with the results of XRD (*vide supra*) showing the two-stage alumination procedure: (1) leaching Ge-atoms from the framework accompanied by the formation of Si–OH defects, followed by (2) incorporation of Al atoms resulting in partial healing of defects.

FTIR spectroscopy of adsorbed pyridine was used to investigate the nature and concentration of acid centers in Al-substituted **UOV** samples. While the intensities of the band of silanol groups (3745 cm^{-1}) slightly decreased after pyridine

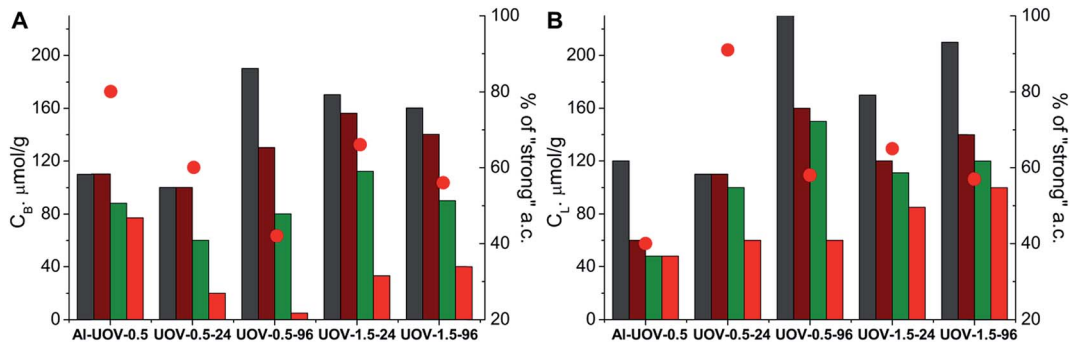

Fig. 7 Concentration of Brønsted (A) and Lewis (B) acid sites for Al-UOV-0.5 and UOV zeolites aluminated at 80 °C for 24 h or 96 h determined based on the desorption of pyridine at different temperatures: 150 °C – ▮, 250 °C – ▮, 350 °C – ▮, 450 °C – ▮. The ratio between the concentration of acid sites determined at 350 °C and 150 °C (in %) is shown as (●).

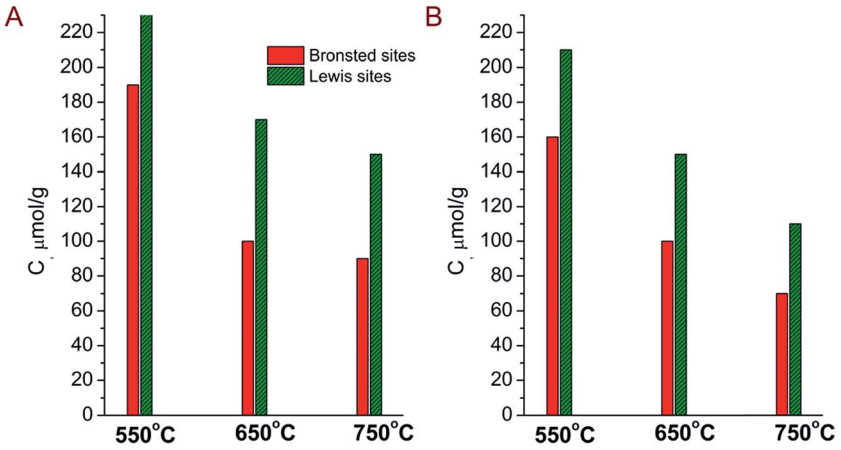

Fig. 8 Concentration of Brønsted and Lewis acid sites for **UOV**-0.5 and **UOV**-1.5 samples treated at 80 °C for 96 h and calcined at different temperatures: 550, 650 and 750 °C.

adsorption, the band assigned to Si–(OH)–Al groups (3620 cm^{-1}) completely disappeared evidencing the accessibility of all Brønsted sites in aluminated samples for the pyridine molecule. Several absorption bands appeared in the region of 1400–1600 cm^{-1} after adsorption of pyridine in Al-containing **UOV** zeolites. An absorption band at 1455 cm^{-1} is characteristic of coordinatively bonded pyridine, while the absorption band at 1545 cm^{-1} is attributed to pyridinium ions adsorbed on Brønsted acid sites (Table 1).

Parent **UOV**-*n* germanosilicates possessed similar small amounts of acid centers (~0.04–0.05 mmol g^{-1}, Table 1). Post-synthesis alumination resulted in a remarkable increase in both the Brønsted (~0.10–0.25 mmol g^{-1}) and the Lewis (~0.11–0.29 mmol g^{-1}) sites for all derivatives.

As discussed previously, the increase in the alumination temperature accelerated the Al incorporation, and thus **UOV**-*n*-Al-175-24h (where $n = 0.5$ and 1.5) samples were characterized by higher total concentrations of acid sites, **UOV**-1.5 (0.34 *vs.* 0.42 µmol g^{-1} for samples aluminated at 80 and 175 °C, respectively) and **UOV**-0.5 (0.21 *vs.* 0.40 mmol g^{-1}). Furthermore, prolongation of the treatment at 80 °C from 24 h to 96 h resulted in the increase in the Lewis site concentration from 0.11–0.17 to 0.21–0.29 mmol g^{-1} (Table 1).

The spectra of Al-**UOV**-*n* samples (Fig. 6III) in the OH-vibration region contained three bands corresponding to silanol defects (3745 cm^{-1}), external Ge–OH and extra-framework Al–OH groups (3676 cm^{-1}) and acidic bridging Si–(OH)–Al (3620 cm^{-1}) groups. Regardless of the chemical composition, samples were characterized by a similar amount of acid sites, namely 0.23 mmol g^{-1} for Al-**UOV**-0.5 and 0.20 mmol g^{-1} for Al-**UOV**-1.5. The amounts of Lewis and Brønsted acid centers in the framework were significantly lower when compared with any of the **UOV**-*n* subjected to post-synthesis alumination, *cf.* ICP-OES analysis (Table SI-1†).

Distribution of acid sites with respect to their strength was investigated by stepwise desorption of pyridine adsorbed on **UOV**-0.5 and **UOV**-1.5 samples subjected to alumination at 80 °C for 24 h and 96 h, and directly synthesized Al-**UOV**-0.5. The

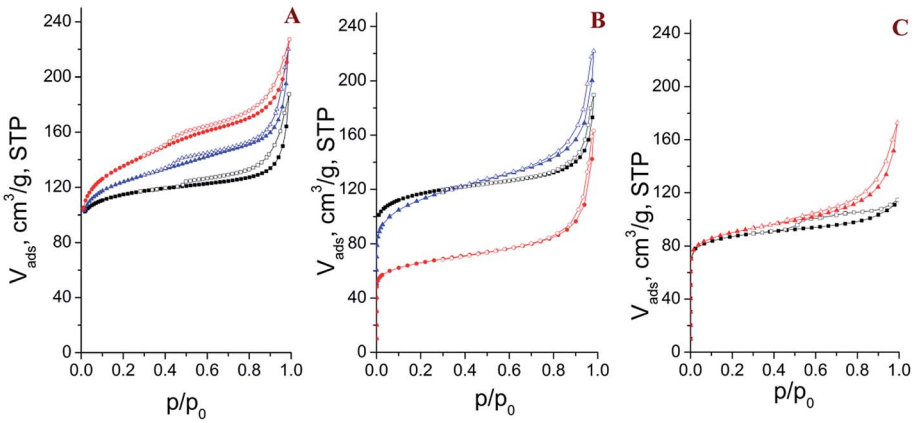

Fig. 9 Nitrogen adsorption and desorption isotherms of (A) **UOV**-1.5 and (B) **UOV**-0.5: initial germanosilicates (black), treated at 80° for 96 h (blue) and at 175 °C for 24 h (red). (C) Nitrogen adsorption and desorption isotherms of Al-**UOV**-*n* samples: Al-**UOV**-1.5 (black) and Al-**UOV**-0.5 (red).

dependence of the concentration of Brønsted and Lewis acid sites occupied by pyridine after desorption at a given temperature and percentage of strong acid centers is presented in Fig. 7. Despite the increase in the total amount of acid sites with the increase of treatment time from 24 h to 96 h, the strength of Brønsted and Lewis acid centers decreased for both **UOV**-0.5 and **UOV**-1.5 samples.

The chemical composition of the starting material and the method of alumination (direct or post-synthesis) control the strength and type of generated acid sites. Although the **UOV**-1.5 sample subjected to post-synthesis alumination was characterized by a comparable fraction of strong acid sites of both types (around 60%), in the case of **UOV**-0.5 the fraction of strong Lewis sites dominated over Brønsted centers (Fig. 7). The maximum value in the case of Lewis sites (91%) was achieved for **UOV**-0.5-Al-80-24h. In contrast to post-synthesis modified materials, the fraction of strong Brønsted sites significantly prevailed over that of Lewis sites for directly synthesized aluminum containing Al-**UOV**-0.5, reaching the value of 80%.

In order to follow the thermal stability of post-synthesis aluminated **UOV** samples, the concentration of acid sites in the **UOV**-*n*-Al-80-96h materials calcined at different temperatures (550, 650 and 750 °C) was measured (Fig. 8). The concentration of both Brønsted and Lewis sites decreased in the order 550° > 650° > 750° indicating a gradual elimination of acid centers with temperature. About 50% of the initial acid sites remained in the sample calcined at elevated temperatures (750 °C).

Textural properties of Al-UOV zeolites: synthesis *vs.* post-synthesis incorporation of Al

Treatments of **UOV** samples with $Al(NO_3)_3$ solution resulted not only in the creation of acid sites, but also in the formation of additional mesopores, that can be used as an advantage for the design of hierarchical porous catalysts. According to the nitrogen adsorption–desorption experiments, parent **UOV**-*n* samples as well as directly synthesized Al-**UOV**-*n* zeolites were characterized by isotherms of type I, but with high uptake in the region of 0.8–1 p/p_0, which is characteristic of interparticle condensation (Fig. 9A–C). The Si/Ge ratio in the parent **UOV** influenced the textural characteristics of the aluminated materials: samples obtained using the Ge-poor zeolite (Si/Ge = 1.5) were characterized by higher mesopore and micropore volumes and surface area (Table 2) if compared with those synthesized by alumination of **UOV**-0.5.

Table 2 Textural properties of UOV samples subjected to direct and post-synthesis alumination

Sample	V_{micro}, $cm^3\ g^{-1}$	V_{meso}, $cm^3\ g^{-1}$	S_{BET}, $m^2\ g^{-1}$
UOV-1.5	0.15	0.12	330
UOV-1.5-Al-80-96h	0.13	0.19	380
UOV-1.5-Al-175-24h	0.12	0.21	420
Al-**UOV**-1.5	0.10	0.06	250
UOV-0.5	0.11	0.21	310
UOV-0.5-Al-80-96h	0.10	0.20	340
UOV-0.5-Al-175-24h	0.07	0.17	200
Al-**UOV**-0.5	0.10	0.15	270

Aluminated **UOV**-1.5 derivatives showed isotherms, which are a combination of types I and IV (Fig. 9A). The mesopore volume and surface area of the samples significantly increased after alumination (Table 2). Such development of porosity is ascribed to non-equivalent replacement of leached framework Ge atoms with Al atoms. Surprisingly, aluminated **UOV**-0.5 derivatives were characterized by micro- and mesopore volumes similar to the parent zeolite. The drop of adsorption parameters for **UOV**-0.5-Al-175-24h is explained by partial degradation of the framework, which is in agreement with the results of XRD and SEM analyses mentioned above.

Al-**UOV**-0.5 and Al-**UOV**-1.5 showed lower micro- and mesopore volumes and BET areas in comparison with **UOV** aluminated by $Al(NO_3)_3$ (Table 2). This difference in adsorption characteristics and the concentration of acid centers between post-synthesis aluminated samples and directly synthesized materials can be considered as an advantage of the post-synthesis approach. Thus, we can control the concentration of acid sites and the *c* (Brønsted sites)/*c* (Lewis sites) ratio by appropriate choice of the chemical composition of the parent **UOV** germanosilicate and post-synthesis treatment conditions.

Conclusions

The present study showed the possibility of post-synthesis substitution of Ge atoms by Al in the framework of germanosilicate **UOV**. The kinetic study of the process showed that Al incorporation is a multi-stage process. On the short times of alumination, we observed acidic hydrolysis of Ge-O-Si bonds accompanied by partial disassembly of the framework and leaching of Ge atoms but with negligible incorporation of Al into the zeolite framework. These findings are in agreement with the results of ICP-OES and ^{27}Al MAS NMR showing a significant increase in Si/Ge ratios and the dominance of signals of extra-framework penta- and hexa-coordinated Al species. In the following step of the procedure, insertion of Al atoms into the structure heals the silanol defects formed after hydrolysis of Ge-domains. Healing of defects was confirmed by ^{29}Si and ^{27}Al MAS NMR, as the spectra of the sample treated for 4 days exhibit significantly decreased intensity attributed to Q^3 silicon atoms and the dominant signal of framework Al in tetrahedral coordination. Furthermore, as it was shown by FTIR spectroscopy, samples treated for longer times were characterized by a decreased intensity of silanol defects along with an increased intensity of bands related to Si–(OH)–Al bridging groups.

Post-synthesis incorporation of Al resulted in the formation of both strong Lewis and Brønsted acid centers. The appropriate choice of the treatment conditions (time and temperature) can be used to control the Brønsted/Lewis acid center ratio, the important parameter for catalytic application. Thus, samples of **UOV**-0.5 and **UOV**-1.5 treated at 80 °C for 4 days had a significantly increased amount of Lewis centers (by 1.7–1.9 times) in comparison with those treated for shorter times. Whereas hydrothermally treated (175 °C) Ge-rich and Ge-poor samples were characterized by a bigger fraction of Brønsted acid centers if we compare with materials aluminated at 80 °C. The intrinsic

properties of parent **UOV** germanosilicates did not significantly influence the total amount of formed acid centers but affected the textural properties of aluminated derivatives. Materials obtained from Ge-poor **UOV**-1.5 were characterized by increased mesopore volume and surface area in comparison with the parent **UOV** zeolite. But in the case of **UOV**-0.5 improvement of textural properties was not observed. The following method of alumination was shown to be appropriate for the design of stable hierarchically porous materials possessing acid centers.

Furthermore, in comparison with direct synthesis of aluminum containing **UOV** zeolites, the post-synthesis treatment was shown to be a more appropriate method for Al incorporation, as it resulted in introduction of a higher amount of framework Al, in the generation of higher amounts of both Brønsted and Lewis acid centers as well as in the development of additional mesoporosity.

Conflicts of interest

There are no conflicts to declare.

Acknowledgements

J. Č. thanks the Czech Science Foundation for the support of the project 17-01440S while M. O. and M. S. acknowledge the same Grant agency for the support (17-06524Y) and M. H. acknowledges financial support from the Deutsche Forschungsgemeinschaft (DFG) in the frame of its cluster of excellence "Engineering of Advanced Materials". M. H. and J. C. thankfully acknowledge financial support from Bayerisch-Tschechische Hochschulagentur (BTHA).

References

1 B. M. Weckhuysen and J. Yu, Recent advances in zeolite chemistry and catalysis, *Chem. Soc. Rev.*, 2015, **44**, 7022–7024.
2 M. E. Davis, Ordered porous materials for emerging applications, *Nature*, 2002, **417**(6891), 813–821.
3 A. Corma, M. T. Navarro, F. Rey, J. Rius and S. Valencia, Pure polymorph C of zeolite beta synthesized by using framework isomorphous substitution as a structure-directing mechanism, *Angew. Chem., Int. Ed.*, 2001, **40**(12), 2277–2280.
4 R. Castañeda, A. Corma, V. Fornes, F. Rey and J. Rius, Synthesis of a new zeolite structure ITQ-24, with intersecting 10-and 12-membered ring pores, *J. Am. Chem. Soc.*, 2003, **125**(26), 7820–7821.
5 A. Corma, M. Puche, F. Rey, G. Sankar and S. J. Teat, A zeolite structure (ITQ-13) with three sets of medium-pore crossing channels formed by 9- and 10-rings, *Angew. Chem., Int. Ed.*, 2003, **42**(10), 1156–1159.
6 N. Bats, L. Rouleau, J. L. Paillaud, P. Caullet, Y. Mathieu and S. Lacombe, Recent developments in the use of hexamethonium salts as structure directing agents in zeolite synthesis, in *Recent Advances in the Science and Technology of Zeolites and Related Materials, Pts a - C*, ed. E. VanSteen, M. Claeys and L. H. Callanan, 2004, vol. 154, pp. 283–288.
7 A. Corma, M. J. Diaz-Cabanas, J. L. Jorda, F. Rey, G. Sastre and K. G. Strohmaier, A Zeolitic Structure (ITQ-34) with Connected 9-and 10-Ring Channels Obtained with Phosphonium Cations as Structure Directing Agents, *J. Am. Chem. Soc.*, 2008, **130**(49), 16482–16483.
8 A. Corma, F. Rey, S. Valencia, J. L. Jorda and J. Rius, A zeolite with interconnected 8-, 10- and 12-ring pores and its unique catalytic selectivity, *Nat. Mater.*, 2003, **2**(7), 493–497.
9 D. L. Dorset, K. G. Strohmaier, C. E. Kliewer, A. Corma, M. J. Diaz-Cabanas, F. Rey and C. J. Gilmore, Crystal Structure of ITQ-26, a 3D Framework with Extra-Large Pores, *Chem. Mater.*, 2008, **20**(16), 5325–5331.
10 J. L. Paillaud, B. Harbuzaru, J. Patarin and N. Bats, Extra-Large-Pore Zeolites with Two-Dimensional Channels Formed by 14 and 12 Rings, *Science*, 2004, **304**(5673), 990–992.
11 A. Corma, M. J. Diaz-Cabanas, F. Rey, S. Nicolooulas and K. Boulahya, ITQ-15: the first ultralarge pore zeolite with a bi-directional pore system formed by intersecting 14- and 12-ring channels, and its catalytic implications, *Chem. Commun.*, 2004, **12**, 1356–1357.
12 J. Jiang, J. L. Jorda, M. J. Diaz-Cabanas, J. Yu and A. Corma, The Synthesis of an Extra-Large-Pore Zeolite with Double Three-Ring Building Units and a Low Framework Density, *Angew. Chem., Int. Ed.*, 2010, **49**(29), 4986–4988.
13 A. Corma, M. J. Diaz-Cabanas, J. Jiang, M. Afeworki, D. L. Dorset, S. L. Soled and K. G. Strohmaier, Extra-large pore zeolite (ITQ-40) with the lowest framework density containing double four- and double three-rings, *Proc. Natl. Acad. Sci. U. S. A.*, 2010, **107**(32), 13997–14002.
14 J. X. Jiang, J. L. Jorda, J. H. Yu, L. A. Baumes, E. Mugnaioli, M. J. Diaz-Cabanas, U. Kolb and A. Corma, Synthesis and Structure Determination of the Hierarchical Meso-Microporous Zeolite ITQ-43, *Science*, 2011, **333**(6046), 1131–1134.
15 G. Sastre, J. A. Vidal-Moya, T. Blasco, J. Rius, J. L. Jordá, M. T. Navarro, F. Rey and A. Corma, Preferential Location of Ge Atoms in Polymorph C of Beta Zeolite (ITQ-17) and Their Structure-Directing Effect: A Computational, XRD, and NMR Spectroscopic Study, *Angew. Chem., Int. Ed.*, 2002, **41**(24), 4722–4726.
16 J. Jiang, J. Yu and A. Corma, Extra-Large-Pore Zeolites: Bridging the Gap between Micro and Mesoporous Structures, *Angew. Chem., Int. Ed.*, 2010, **49**(18), 3120–3145.
17 R. Castañeda, A. Corma, V. Fornes, J. Martinez-Triguero and S. Valencia, Direct synthesis of a 9 × 10 member ring zeolite (Al-ITQ-13): a highly shape-selective catalyst for catalytic cracking, *J. Catal.*, 2006, **238**(1), 79–87.
18 T. Blasco, A. Corma, M. J. Diaz-Cabanas, F. Rey, J. A. Vidal-Moya and C. M. Zicovich-Wilson, Preferential location of Ge in the double four-membered ring units of ITQ-7 zeolite, *J. Phys. Chem. B*, 2002, **106**(10), 2634–2642.
19 G. Sastre, A. Pulido, R. Castañeda and A. Corma, Effect of the Germanium Incorporation in the Synthesis of EU-1,

ITQ-13, ITQ-22, and ITQ-24 Zeolites, *J. Phys. Chem. B*, 2004, **108**(26), 8830–8835.

20 W. J. Roth, P. Nachtigall, R. E. Morris, P. S. Wheatley, V. R. Seymour, S. E. Ashbrook, P. Chlubna, L. Grajciar, M. Polozij, A. Zukal, O. Shvets and J. Cejka, A family of zeolites with controlled pore size prepared using a top-down method, *Nat. Chem.*, 2013, **5**(7), 628–633.

21 W. J. Roth, O. V. Shvets, M. Shamzhy, P. Chlubna, M. Kubu, P. Nachtigall and J. Čejka, Postsynthesis Transformation of Three-Dimensional Framework into a Lamellar Zeolite with Modifiable Architecture, *J. Am. Chem. Soc.*, 2011, **133**(16), 6130–6133.

22 P. Eliášová, M. Opanasenko, P. S. Wheatley, M. Shamzhy, M. Mazur, P. Nachtigall, W. J. Roth, R. E. Morris and J. Čejka, The ADOR mechanism for the synthesis of new zeolites, *Chem. Soc. Rev.*, 2015, **44**, 7177–7206.

23 M. Mazur, P. S. Wheatley, M. Navarro, W. J. Roth, M. Položij, A. Mayoral, P. Eliášová, P. Nachtigall, J. Čejka and R. E. Morris, Synthesis of 'unfeasible' zeolites, *Nat. Chem.*, 2016, **8**, 58–62.

24 V. I. Kasneryk, M. V. Shamzhy, M. V. Opanasenko and J. Cejka, Tuning of textural properties of germanosilicate zeolites ITH and IWW by acidic leaching, *J. Energy Chem.*, 2016, **25**(2), 318–326.

25 L. Burel, N. Kasian and A. Tuel, Quasi All-Silica Zeolite Obtained by Isomorphous Degermanation of an As-Made Germanium-Containing Precursor, *Angew. Chem., Int. Ed.*, 2014, **53**(5), 1360–1363.

26 X. L. Liu, N. Kasian and A. Tuel, New insights into the degermanation process of ITQ-17 zeolites, *Microporous Mesoporous Mater.*, 2014, **190**, 171–180.

27 M. V. Shamzhy, P. Eliasova, D. Vitvarova, M. V. Opanasenko, D. S. Firth and R. E. Morris, Post-Synthesis Stabilization of Germanosilicate Zeolites ITH, IWW, and UTL by Substitution of Ge for Al, *Chem.–Eur. J.*, 2016, **22**(48), 17377–17386.

28 M. Shamzhy and F. S. d. O. Ramos, Tuning of acidic and catalytic properties of IWR zeolite by post-synthesis incorporation of three-valent elements, *Catal. Today*, 2015, **243**, 76–84.

29 M. V. Shamzhy, M. V. Opanasenko, F. S. D. Ramos, L. Brabec, M. Horacek, M. Navarro-Rojas, R. E. Morris, H. D. Pastore and J. Cejka, Post-synthesis incorporation of Al into germanosilicate ITH zeolites: the influence of treatment conditions on the acidic properties and catalytic behavior in tetrahydropyranylation, *Catal. Sci. Technol.*, 2015, **5**(5), 2973–2984.

30 M. V. Shamzhy, C. Ochoa-Hernandez, V. I. Kasneryk, M. V. Opanasenko and M. Mazur, Direct incorporation of B, Al, and Ga into medium-pore ITH zeolite: synthesis, acidic, and catalytic properties, *Catal. Today*, 2016, **277**, 37–47.

31 F. Gao, M. Jaber, K. Bozhilov, A. Vicente, C. Fernandez and V. Valtchev, Framework Stabilization of Ge-Rich Zeolites *via* Postsynthesis Alumination, *J. Am. Chem. Soc.*, 2009, **131**(45), 16580–16586.

32 W. H. Fu, Z. Q. Yuan, Z. D. Wang, Y. D. Wang, W. M. Yang and M. Y. He, Direct synthesis of hydrothermally stable Ge-IWR zeolites, *Dalton Trans.*, 2017, **46**(20), 6692–6699.

33 N. Zilkova, M. Shamzhy, O. Shvets and J. Cejka, Transformation of aromatic hydrocarbons over isomorphously substituted UTL: comparison with large and medium pore zeolites, *Catal. Today*, 2013, **204**, 22–29.

34 H. Xu, J.-g. Jiang, B. Yang, L. Zhang, M. He and P. Wu, Post-Synthesis Treatment gives Highly Stable Siliceous Zeolites through the Isomorphous Substitution of Silicon for Germanium in Germanosilicates, *Angew. Chem., Int. Ed.*, 2014, **53**(5), 1355–1359.

35 Y. Lorgouilloux, M. Dodin, E. Mugnaioli, C. Marichal, P. Caullet, N. Bats, U. Kolb and J.-L. Paillaud, IM-17: a new zeolitic material, synthesis and structure elucidation from electron diffraction ADT data and Rietveld analysis, *RSC Adv.*, 2014, **4**(37), 19440–19449.

36 V. Kasneryk, M. Shamzhy, M. Opanasenko, P. S. Wheatley, S. A. Morris, S. E. Russell, A. Mayoral, M. Trachta, J. Cejka and R. E. Morris, Expansion of the ADOR Strategy for the Synthesis of Zeolites: The Synthesis of IPC-12 from Zeolite UOV, *Angew. Chem., Int. Ed.*, 2017, **56**(15), 4324–4327.

37 S. Brunauer, P. H. Emmett and E. Teller, Adsorption of Gases in Multimolecular Layers, *J. Am. Chem. Soc.*, 1938, **60**(2), 309–319.

38 B. C. Lippens and J. H. de Boer, Studies on pore systems in catalysts: V. The t method, *J. Catal.*, 1965, **4**(3), 319–323.

39 C. A. Emeis, Determination of Integrated Molar Extinction Coefficients for Infrared-Absorption Bands of Pyridine Adsorbed on Solid Acid Catalysts, *J. Catal.*, 1993, **141**(2), 347–354.

40 J. A. Vidal-Moya, T. Blasco, F. Rey, A. Corma and M. Puche, Distribution of fluorine and germanium in a new zeolite structure ITQ-13 studied by F-19 nuclear magnetic resonance, *Chem. Mater.*, 2003, **15**(21), 3961–3963.

41 X. Ren, J. Liu, Y. Li, J. Yu and R. Xu, Hydrothermal synthesis of an ITH-type germanosilicate zeolite in a non-concentrated gel system, *J. Porous Mater.*, 2013, **20**(4), 975–981.

42 G. Metz, X. L. Wu and S. O. Smith, *J. Magn. Reson., Ser. A*, 1994, **110**, 219–227.